Paper # G38 Topic: Modeling

5th US Combustion Meeting
Organized by the Western States Section of the Combustion Institute
And Hosted by the University of California at San Diego
March 25-28, 2007

Computational fluid dynamics modeling of the operation of a flame ionization sensor

E. David Huckaby, Benjamin Chorpening and Jimmy Thornton

U.S. Department of Energy, National Energy Technology Laboratory
Morgantown, West Virginia, 26507-0880, USA

The sensors and controls research group at the United States Department of Energy (DOE) National Energy Technology Laboratory (NETL) is continuing to develop the Combustion Control and Diagnostics Sensor (CCADS) for gas turbine applications. CCADS measures the electrical conduction of the charged species generated during the combustion process to detect flashback and combustion instabilities, and to monitor equivalence ratio. As part of this effort, combustion models are being developed which include the interaction between the electric field and the transport processes of the charged species. The primary combustion process is computed using a flame wrinkling model developed by Weller et al. (1998). A sub-model for the transport of charged species is *attached* to this model. The formulation of the charged-species model is similar to that applied by Penderson and Brown (1993) for the simulation of laminar flames. Using the above procedure, numerical simulations are performed and the results are compared with experimental current measurements. Quantitative agreement with experiment was not obtained, however the model does display similar sensitivity to flow and operating conditions as observed in experiments.

1 Introduction

The United States Department of Energy (DOE) National Energy Technology Laboratory (NETL) conducts programs that support the global interest for clean and efficient power generation such as the Turbine Program. In support of the goals of the Turbine Program, NETL's sensors and controls research group is continuing to develop the Combustion Control and Diagnostics Sensor (CCADS) for gas turbine applications. This sensor development is based on using the flame's electrical properties to perform real-time diagnostics and in-situ monitoring of critical combustion parameters. This paper describes the development of a model and ongoing research on ion and electron distribution in a lean premixed turbulent combustor, which supports this sensor development effort. Previous experiments at NETL with premixed combustors have demonstrated that the current signal can be potentially processed to: (1) detect flash-back (Thornton et al., 2000), (2) determine the primary acoustic (combustion dynamics) frequencies (Straub et al., 2002), (3) detect incipient lean blow-off (Bensen et. al. 2005) (4) determine relative amplitudes acoustic waves (combustion dynamics) (Chorpening et al., 2004), (5) determine equivalence ratio (Straub et al., 2002).

This paper discusses a model developed at NETL to integrate the electric field emanating from CCADS electrodes with the lean premixed combustion process and ion reaction/transport sub-models to simulate CCADS sensor test results. The primary combustion process is computed using a flame wrinkling model (Weller et al., 1998) which is a component of the OpenFOAM

toolkit (Jasak et. al. 2004). A sub-model for the transport of charged species is *attached* to this model. The formulation of the charged-species model is similar to that applied by Penderson and Brown (1993) for the simulation of laminar flames. The goal is to use the results of numerical simulation to aid interpretation of the current signals which result from the interaction of a turbulent flame and an electric field.

Several researchers have used a variety of numeric approaches to model flame ionization. Of the previous numerical modeling of flame ions, there have been several simulation of stirred-reactor systems [Aithal, et. al. 1999, Mehresh, et. al. 2005], a simulation of an opposed flow flame [Jones et. al. 1972], multiple freely-propagating-one-dimensional flame simulations [Brown and Erslan 1988, Erslan and Brown 1998, Penderson and Brown 1993, Prager 2005, Prager et. al. 2007] , a one dimensional simulation to investigate flame speeds enhancement by microwave heating [Ju et. al. 2004] and a study comparing burner stabilized flame simulations with experiments [Lilly 2007]. In addition, Hu et. al [2000] have simulated the effects of electric fields on laminar premixed and non-prefmixed "candle" flames in two dimensions. Of the noted flame ionization simulation work, little has been done to model ion transport in multidimensional turbulent flames. This is an essential part to effectively model and understand CCADS results in lean premixed combustion applications such as advanced dry low emission gas turbines. The model development at NETL and described herein includes the ion-transport modeling as part of the turbulent multidimensional flame simulations. The simulation also differs from the other investigation, because the primary combustion process is not calculated using a chemical kinetic model. The sub-model for ion transport, which is formulated below, is a combination of the one dimensional model for ions in flames proposed by Penderson and Brown [1993] with some additional numerical techniques used by Haglelaar [2000].

2 Model Description

2.1 Primary Combustion Process

The bulk flow and combustion process is modeled by the compressible Reynolds-averaged Navier Stokes (RANS) equations augmented with the flame-wrinkling model of Weller et al. [1993, 1998]. An implementation called *XiFoam* of these equations is available as part of OpenFOAM version 1.3 [2006]. The equation set consists of the Favre-averaged conservation of mass, momentum and energy. The Renormalization Group Theory (RNG) k- ε turbulence model is used to model the Reynolds stresses. The turbulent heat and species fluxes are calculated using a gradient diffusion model with unity turbulent Prandtl and Schmidt numbers. The flame wrinkling model adds four additional transported scalars, the regress variable, b, the flame-wrinkling, Ξ, the fuel fraction, $f_{t,}$ and the strained laminar flame speed, $S_{u,}$ to the system.

2.1 Charged Species Transport

There is no numerical feedback (chemical, thermal or mechanical) from the ion-transport model to the bulk flow; thus, it cannot be used to describe flame manipulation by an electric field. However, the electric field used in CCADS is much weaker than that typically used in flame manipulation strategies, so the field is not expected to have a significant effect on the combustion. Not allowing the electric field to modify the flame in the model provides numerical

efficiencies of significant benefit in a multidimensional simulation.

The ion transport model consists of a set of transport/reaction equations for the concentration of the considered charged species:

$$\frac{\partial}{\partial t}\left(C_k\right)+\nabla\cdot\left(\vec{u}C_k+J_k\right)=P_{ion}-D_{ion},$$

and Gauss's law to determine the electric potential, φ,

$$-\nabla^2\varphi=\left(\frac{N_A q}{\varepsilon_0}\right)\sum z_k C_k,$$

where k is the index of the ion concentration vector, which consists in this work of only electrons and hydronium ions ($H3O^+$). Further ε_0 is the permittivity of free space, q is the magnitude of the charge of an electron, and N_A is Avogadro's Constant.

The non-convective species flux is calculated using the drift-flux approximation. Applying this model this flux is split into two terms:

$$J_k=-z_k b_k C_k\nabla\phi-D_k\nabla C_k$$

The first term, the drift flux, accounts for the influence of the electric field and second the flux due to concentration gradients. Thermal diffusion, which could be a significant method of electron transport, has been neglected. The drift-flux model is in contrast to modeling the non-convective flux through either a multi-component diffusion model or calculating the total species flux by a momentum balance for each species, as is done with a multi-fluid model [Bukowski et. al. 1996]. A further assumption of the model is that the electrons are in thermal equilibrium with the surrounding gas and thus a separate energy equation for the electrons is not necessary. [Smirnov 2001].

The mixture-averaged diffusivity is calculated from the viscosity of the bulk flow using a constant Schmidt number, $Sc_k=\mu(T)/(\rho D_k)$, for each species. The mobility of the charged species, b_k is related to the species diffusivity using Einstein's relation [Smirnov 2001]:

$$b_k=D_k\left(\frac{q}{k_B T}\right)$$

The Schmidt number for the heavy species is unity, while a Schmidt number of 0.006 is used for the electrons. The Schmidt number was calculated to give an electron mobility of 0.4 (m/s)/(V/m) [Goodings et. al., 2001] at 2000 K and atmospheric pressure with the viscosity calculated using Sutherland's law for air. The electron mobility and diffusivity calculated using this procedure can be considered representative of more accurate values [Fialakov 1997]. However, due to the relatively large values of the laminar transport properties, a more rigorous treatment of the electron transport might be warranted, such as using collision integrals [Selle and Riedel 2007, Wright et. al. 2005], polynomial fits of the binary diffusion coefficients [Svehla 1995] or direct calculation using a Boltzmann equation [Ju et. al 2004, Subramaniam 2005, Sakhrieh et. al. 2005].

Finally, the two governing equations are Reynolds (ensemble) averaged to obtain equations

compatible with the URANS simulation technique [Poinsot and Veynante 2001]. After averaging, the species conservation equations become

$$\frac{\partial}{\partial t}\left(\overline{C}_k\right)+\nabla\cdot\left(\overline{\vec{u}}\,\overline{C}_k+\overline{J_k}+J_{t,k}\right)=\overline{P}_{ion}-\overline{D}_{ion}$$

Gauss's Law is linear and thus the fluctuations of the flow variables do not appear in the equation.

The turbulent species flux, $J_{t,k}$, is calculated using a gradient diffusion model,

$$J_{t,k}=-\frac{\mu_t}{\rho Sc_t}\nabla\overline{C}_k\,,$$

with the turbulent Schmidt number of unity, $Sc_t=1$, as with the other transported scalars in the system. The correlation of the fluctuating species concentrations and electric field gradient $\left(\overline{c_k'\nabla\varphi'}\right)$ are neglected as are the fluctuations of the species mobility and diffusivity. With these simplifications the expression for the laminar species flux has the same functional form as the laminar flux,

$$\overline{J}_k=-D_k\nabla\overline{C}_k-b_k z_k\overline{C}_k\nabla\overline{\varphi},$$

with ensemble averages replacing the instantaneous values.

2.2 Ion Reaction Model

Two assumptions are used to determine the production rates of the two ions considered in the model. First is that the ratio of the average rate of the primary ion production reaction,

$CH+O\Rightarrow HCO^{+}+e^{-}$,

to the overall fuel destruction rate is independent of the effects of turbulence (and strain). The second assumption is that the charge transfer reaction,

$HCO^{+}+H_2O\Rightarrow H_3O^{+}+CO$,

occurs instantaneously and consequently the transport of the formyl cation (HCO^{+}) can be neglected.

The first assumption allows one to approximate the production of ions (e- and HCO+) in the flame by the product of the fuel destruction rate and a differential factor which is a generalization of the *carbon count rule (CCR)* used to calibrate a flame ionization detector (Fialkov[1997], Holm [1999])

$$P_{ion}=-\left(CCR\right)\overline{\dot{\omega}}_F$$

where $\overline{\dot{\omega}}_F$ is the net reaction rate of the fuel. In the context of the flame-wrinkling model, this is taken from the source term of the regress variable, b, and can be written as

$$P_{ion}=\left(CCR\right)\frac{f_t}{W_F}\rho_u S_u\Xi\left|\nabla b\right|$$

The carbon count rule is assumed to be a property of flame as a whole, similar to the laminar flame speed, thus for a given fuel it is calculated from the unburnt mixture temperature, the operating pressure and the equivalence ratio (or fuel fraction)

$$CCR = CCR\left(T_u, p, \Phi\left(f_t\right)\right)$$

The ratio can be determined experimentally or by simulation. With the assumption that ions are only produced by the reaction of methyl radicals and elemental oxygen, the ratio can be calculated as:

$$CCR = \frac{\int k_{ion}[CH][O]dz}{-\int \dot{\omega}_F dz} = \frac{\int k_{ion}[CH][O]dz}{\rho S_u Y_F / W_F}.$$

The freely propagating laminar flame code in Cantera version 1.7 [Goodwin 2006] is used with GRI-Mech 3.0 to calculate the species concentrations, fuel reaction rate and flame speed. The pre-exponential factor was initially calculated using the expression [Prager et al. 2007],

$$k_{ion} = 2.51\times10^{11}\exp\left(-3.61\left(K\right)/T\right)cm^3/mol/s.$$

The expression was later corrected to the following:

$$k_{ion} = 2.51\times10^{11}\exp\left(-856\left(K\right)/T\right)cm^3/mol/s.$$

Figure 1 shows a plot of the production ratio, CCR, at the conditions which were simulated (533K and 2.1 atm). The curve labeled "GRI 3.0" uses the first equation, while the curve labeled "GRI 3.0 corr" uses the second. For reference, the ratio calculated from a simulation with the University of Delaware Mechanism [Qin et. al., 2000] and the first expression is also shown. All the values are less than the values (~10^{-6}) used for flame ionization detectors. Other expressions for this reaction rate are available in the literature (Aithal et al. [1999] , Jones et. al. [1972], Penderson and Brown [1993], etc.) and should produce similar qualitative results. Additional improvement in the estimate of this quantity could be obtained by supplementing a base hydrocarbon oxidation model with a more detailed set of CH and O reactions. [Ju et. al. 2004, Smith et. al. 2002]

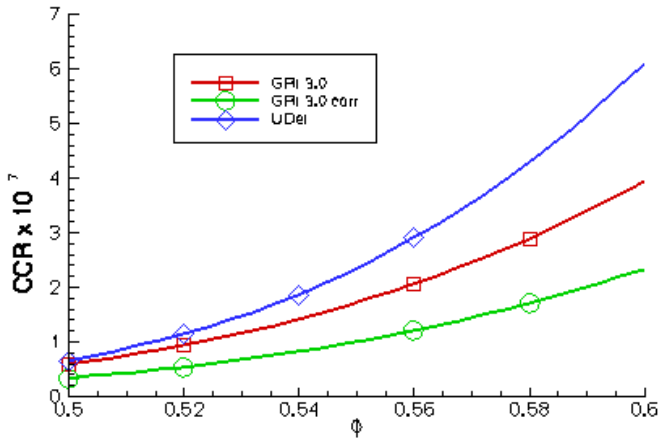

Figure 1- Variation of the Carbon Count Constant at 2.1 atm and 533K

The final part of the ion-reaction model is the recombination the electrons and hydronium, which is assumed to proceed at the unstrained laminar reaction rate. The simulations in this work use the rate expression used by Jones et. al [1972]:

$$D_{ion} = 1.44\times10^{17}\left[H3O^{+}\right]\left[e^{-}\right]$$

As with the expression for the ionization reaction rate coefficient, several other options exist in the literature.

3 Numerical Method

The introduction of ions into the system of equations introduces the following two time scales

$$\tau_k = \frac{\Delta}{u_k} = \frac{\Delta}{u - b_k z_k \nabla\varphi} \qquad \tau = \frac{\varepsilon_0}{\sigma} = \frac{\varepsilon_0}{N_A q \sum b_k |z_k|}$$

where Δ is the local grid spacing. The first is time scale is the cell residence time of the charged species k and the second is the dielectric relaxation time of the system associated with the mutual attraction/repulsion of the charged particles [Hayt 1986]. Either scale, particularly the second, can be smaller than the convective time-scales of the bulk flow and thus could impose a constraint on the allowable time step. To facilitate a tractable simulation time, a fully implicit procedure is selected for the ion model and is implemented by a predictor/corrector iteration over the species conservations equations and Guass's Law. The formulation of the corrector is taken from Haglaar [2000] and is required to address the instability associated with the dielectric relaxation time in the context of a segregated solution algorithm.

The predictor step consists of an implicit solution of the ion concentration using the electric potential from the previous iteration and the bulk flow field at the new time step

$$\frac{C_k^{m+1/2} - C_k^n}{\Delta t} + \nabla\cdot\left(u^{n+1}C_k^{m+1/2} - z_k b_k C_k^{m+1/2}\nabla\varphi^m - D_{k,eff}\nabla C_k^{m+1/2}\right) = P_{ion}^{n+1} - D_{ion}^m$$

where the iteration index is denoted by "*m*" and the time step index by "*n*". This is followed by a corrector step, in which only the potential, ϕ, is treated implicitly

$$\frac{C_k^{m+1} - C_k^n}{\Delta t} + \nabla\cdot\left(u^{n+1}C_k^{m+1/2} - z_k b_k C_k^{m+1/2}\nabla\varphi^{m+1} - D_{k,eff}\nabla C_k^{m+1/2}\right) = P_{ion}^{n+1} - D_{ion}^m$$

$$-\nabla^2\varphi^{m+1} = \left(\frac{N_A q}{\varepsilon_0}\right)\sum z_k C_k^{m+1} \,.$$

The corrector -step minus the predictor step yields the following equation for concentration after the predictor step:

$$\frac{C_k^{m+1} - C^{m+1/2}}{\Delta t} + \nabla\cdot\left(-z_k b_k C_k^{m+1/2}\nabla\left(\varphi^{m+1} - \varphi^m\right)\right) = 0$$

This is substituted into equation for the electrostatic potential to yield an equation for the potential increment, $\delta\varphi = \varphi^{m+1} - \varphi^m$,

$$-\nabla^2\left(\delta\varphi\right) - \frac{\Delta t}{\varepsilon_0}\nabla\cdot\left(\hat{\sigma}\nabla\delta\varphi\right) = \left(\frac{N_A q}{\varepsilon_0}\right)\sum_k z_k C_k^{m+1/2} + \nabla^2\varphi^m \,,$$

where the expression, $\hat{\sigma} = N_A q\sum_k z_k^2 b_k C_k^{m+1/2}$ is used to calculate the conductivity. The predictor-corrector continues for specified number of iteration and/or error tolerance. The results shown

prescribe a maximum of 10 iterations and an error tolerance on Gauss's equation residual of 10^{-4}.

4 Experiments

Numerical simulations were performed similar to a set of experiments conducted in the Simulation Validation (*SimVal)* combustor (Figure 2) in the Spring of 2006. The SimVal facility includes a high-pressure, optically-accessible test section; natural gas, hydrogen, and preheated (non-vitiated) air supply systems; and an exhaust gas sampling system. The combustor is similar in size to a commercial gas turbine combustor, and can operate at pressures and temperatures of relevance to gas turbines. The inlet section of SimVal is normally configured with air and fuel mixing upstream of a perforated plate, which chokes the inlet flow to isolate the combustion chamber from upstream system acoustics. A slotted swirler positioned downstream of the choke plate applies swirl to the flow as it moves around the centerbody and through the remainder of the premix passage to the optically-accessible dump combustor section. Additional combustor and test facility details are discussed elsewhere [Sidwell, 2006]. For these tests a 20 degree slotted swirler is used (shown in the top left of Figure 2), however the flow through the swirler was not included in this study.

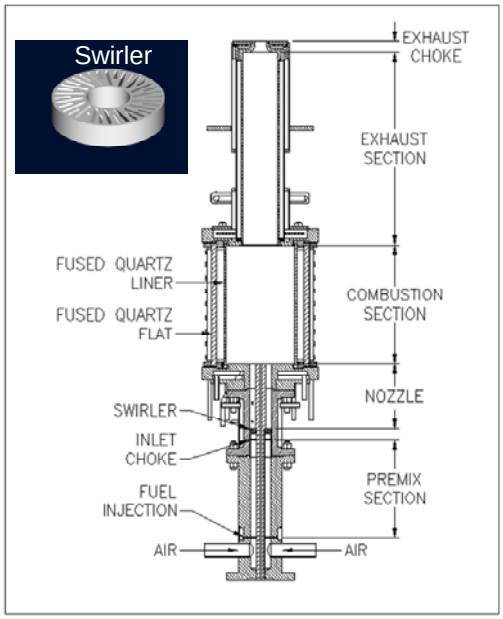

Figure 2 – Schematic of the Simulation Validation (SimVal) Combustor

The end of the CCADS centerbody which was used for these tests is shown in Figure 3. The "sense" electrode consists of section of the centerbody between the two insulating rings. The "guard" electrode consists of the metal surface downstream of the insulating rings, and includes the entire front surface (tip) of the centerbody. The terms "guard" and "sense" are derived from use of CCADS as a flashback sensor. During normal operation, the potential field from the guard electrode prevents the sense from measuring current; however, during flashback the flame moves into the premixer past the guard, producing ions and electrons in the potential field of the sense electrode, allowing it to conduct current to the wall of the premixer. The flow passages through

the tip of the centerbody are used for both cooling air and for piloting.

Figure 3: Photograph of the centerbody with attached CCADS electrodes.

The full experimental matrix consists of an range of equivalence ratios between 0.5 to 0.6, nominal velocities of 40, 60, and 80 m/s and operating pressures of 2.1, 4.2, and 8.4 atm all with 533K preheated air. Pipeline natural gas was used as the fuel. The simulations described in the next section are of the low pressure (2.1 atm) low velocity (40 m/s) tests at equivalence ratios of 0.5 and 0.6. These are performed with and without centerbody piloting.

5 Computational Model

The experiments were simulated using an axisymmetric geometry. The grid for the SimVal experiment is shown in Figure 4, which consists of about thirty thousand grid cells. The circular cooling holes are approximated by a notch on the centerbody at the approximate radius of the center of a cooling hole (Figure 5). The center of the notch is aligned with the centerline of the pilot fuel holes and constructed to with an area equivalent to that of the holes. As a result, the notch can provide the same flow but will not provide the same momentum as the actual pilot jects. Furthermore the "guard" electrode is split into two parts: the front surface of the centerbody and the outer surface downstream of the last insulation ring. A significant portion of both the premixed injector and the exhaust section are not included in the simulations.
For simplicity the pipeline natural gas is approximated by pure methane. This will have some effect on the results since the presence of higher hydrocarbons would tend to increase the flame speed and increase ion yield for a given amount of fuel. However, the error introduced by this is expected to be inconsequential relative to the other modeling assumptions.

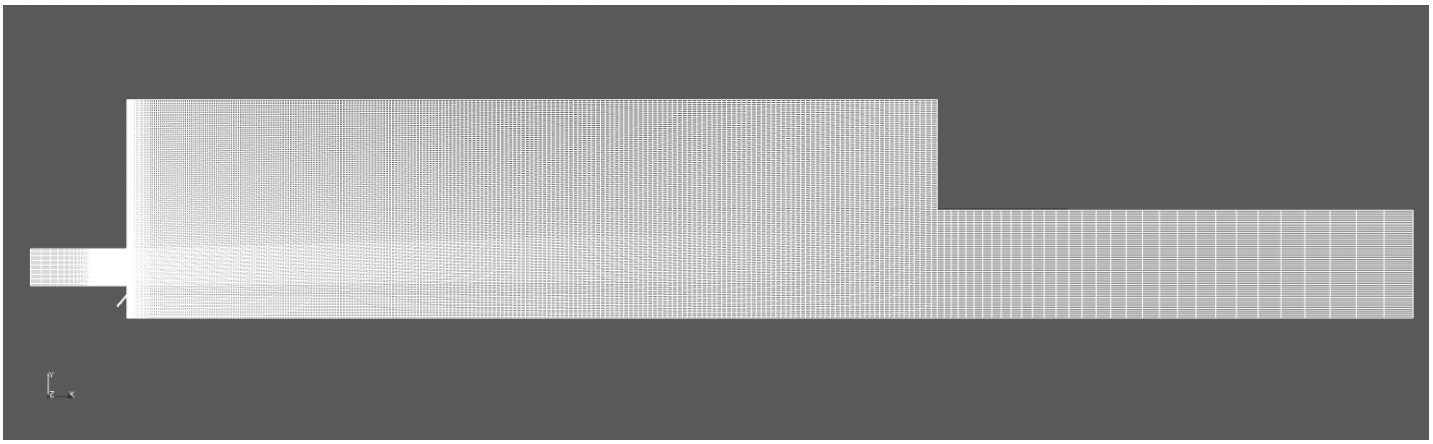

Figure 4 – Computational Mesh

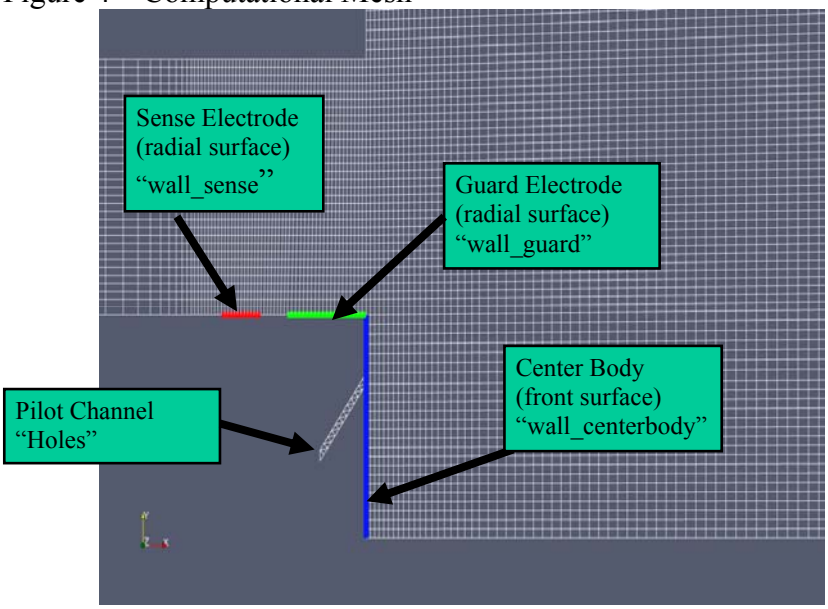

Figure 5 – Mesh near Centerbody, Detail of electrodes and pilot hole.

The simulations which were performed and input conditions are summarized in Tables I and II. The tangential inlet velocity was calculated assuming the flow was turned by exactly the angle of the swirl vanes, 20 degrees. More detailed specification of inlet condition is left for future work. Also the simulations were performed with adiabatic combustor walls. Accounting for heat losses would be expected to reduce the flame temperature and thus reduce the calculated current levels.

Table I – Summrary of Simulations

Condition	Φ	Piloting	Ignition	Outer Wall	Sc_e	CCR
1	0.5	yes	Injector	Grounded	0.006	uncorrected
2	0.5	no	"	"		"
3	0.6	yes	"	"		"
4	0.6	no	Injector	"		"
5	0.5	yes	Combustor	Grounded		"
6	0.5	yes	Injector	Insulated	0.006	"

7	0.5	yes	"	Grounded	0.003	"
8	0.5	yes	"	"	0.006	uncorrected
9	0.5	yes	"	"	"	corrected

Table II – Simulation Conditions – Fixed Parameters

Outlet Pressure	2.1 atm (15 psig)
Inlet Temperature	533 K
Axial Velocity (Main)	40 m/s
Tangential Velocity (Main)	14.4 m/s
Velocity (Pilot Inlet)	92.3 m/s
Velocity (Pilot Combustor)	~40 m/s
Electrode Potential	100 V
Combustor Walls	0 V

All the transport equations are discertized in space using a finite volume method and discretized in time using backward Euler. Laplacian-like terms are calculated using 2^{nd}-order central differences. The PISO algorithm is used for the bulk flow along with a 2^{nd}-order gradient-limited space discretization for the convective terms. The equations for the ions in contrast discretize the convective terms using a 1^{st}-order upwind method for the combined drift and bulk velocity. The effect of the discretization scheme on the results and model behavior is planned in future work.

6 Results

6.1 Initial Condition

The simulations are initiated by first running a cold flow simulation with air to produce a somewhat realistic velocity field. For all but one the simulations (number 5 of Table I), the combustion is then initialized with a flame located at the exit plane of injector (Figure 6). This is done by initializing the regress variable, *b*, to 1 on the inlet side and 0 on the exit side of the dump plane, and analogously setting the temperature to inlet value and the adiabatic flame temperature. An alternative initialization strategy was also tried (Figure 6) in which a "flame sheet" is assumed to protrude from centerbody into the combustor at an arbitrary angle.

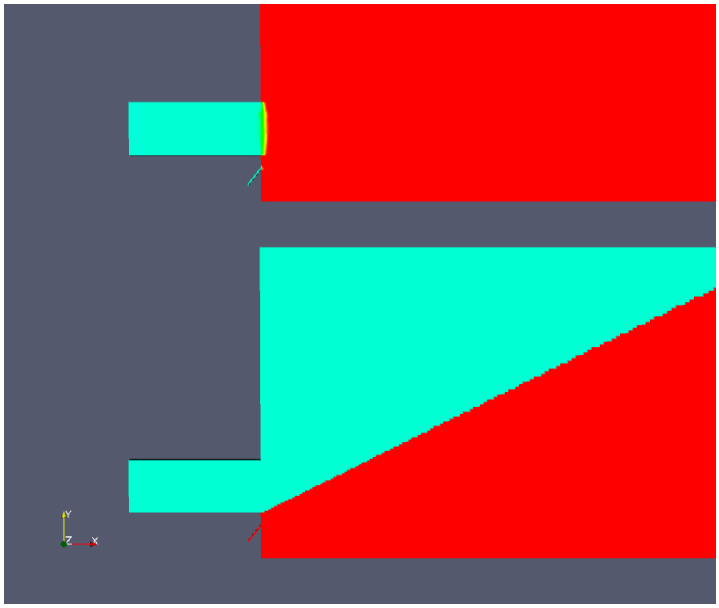

Figure 6 – Initial Temperature Contours for two different initialization strategies
blue: unburnt and 533K, red: burnt and 1650K
top: simulations 1-4 and 6-9, bottom: simulation 5,

6.2 Equivalence Ratio and Piloting

The current histories of the first four simulations of Table I (Figure 7), show that the current increases with equivalence ratio and fuel piloting. The large scale oscillations in the $\Phi = 0.6$, fuel piloted case are due to a numerical instability which will be discussed in *Section 6.4*. The current increasing with equivalence ratio is not surprising given that ion production rate increase with equivalence ratio. The piloted simulations exhibit higher current than the un-piloted cases due to a combination of continued flame attachment and a region high ion concentration in the vicinity of the electrode, which can be seen by the electron concentrations. (Figure 9 a-d). The calculated currents, between 2 mA and 30 μA compare with experimental average current measurements between 250 μA and 30 μA (Figure 8). The air piloted cases appear to be decreasing in current, so the limit-cycle currents will likely be lower than the experimental values. The piloted simulations in contrast clearly over-predict the current ratio.

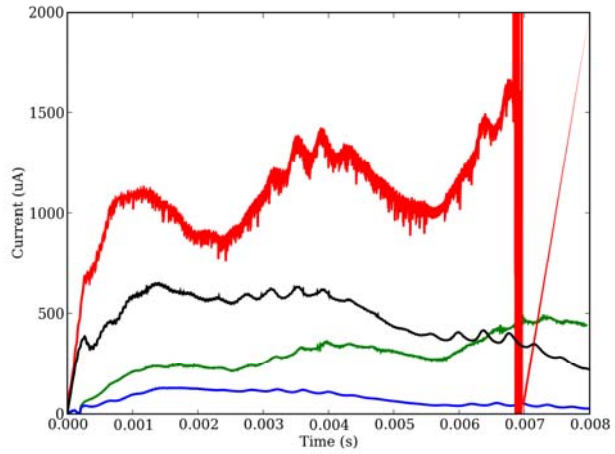

Figure 7 – Guard Current
green: pilot, Φ = 0.5; blue: no pilot Φ = 0.5; red: pilot, Φ = 0.6, black: no pilot, Φ = 0.6

Experimentally, the current at an equivalence ratio of 0.6 was measured about 3.6 times higher than the current at an equivalence ratio of 0.5 for the piloted case. This ratio increased to 4.1 for the un-piloted case. Figure 10 compares this ratio for the piloted and un-piloted simulations with the experimental values. The piloted cases, which have the same flame structure, reproduce the experimental ratio varying between 3.4 and 4. In contrast the un-piloted simulations have a much higher ratio, due to the flame of low equivalence ratio simulation detaching from the center body at earlier time the flame of the high equivalence ratio simulation..

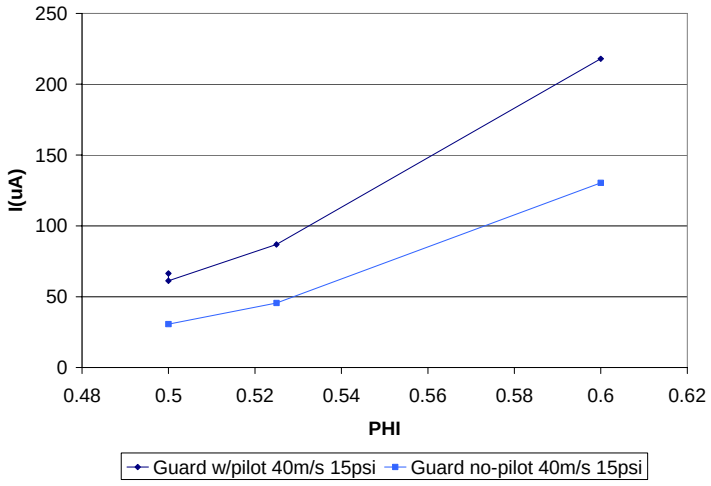

Figure 8 – Experimental Current Measuremen

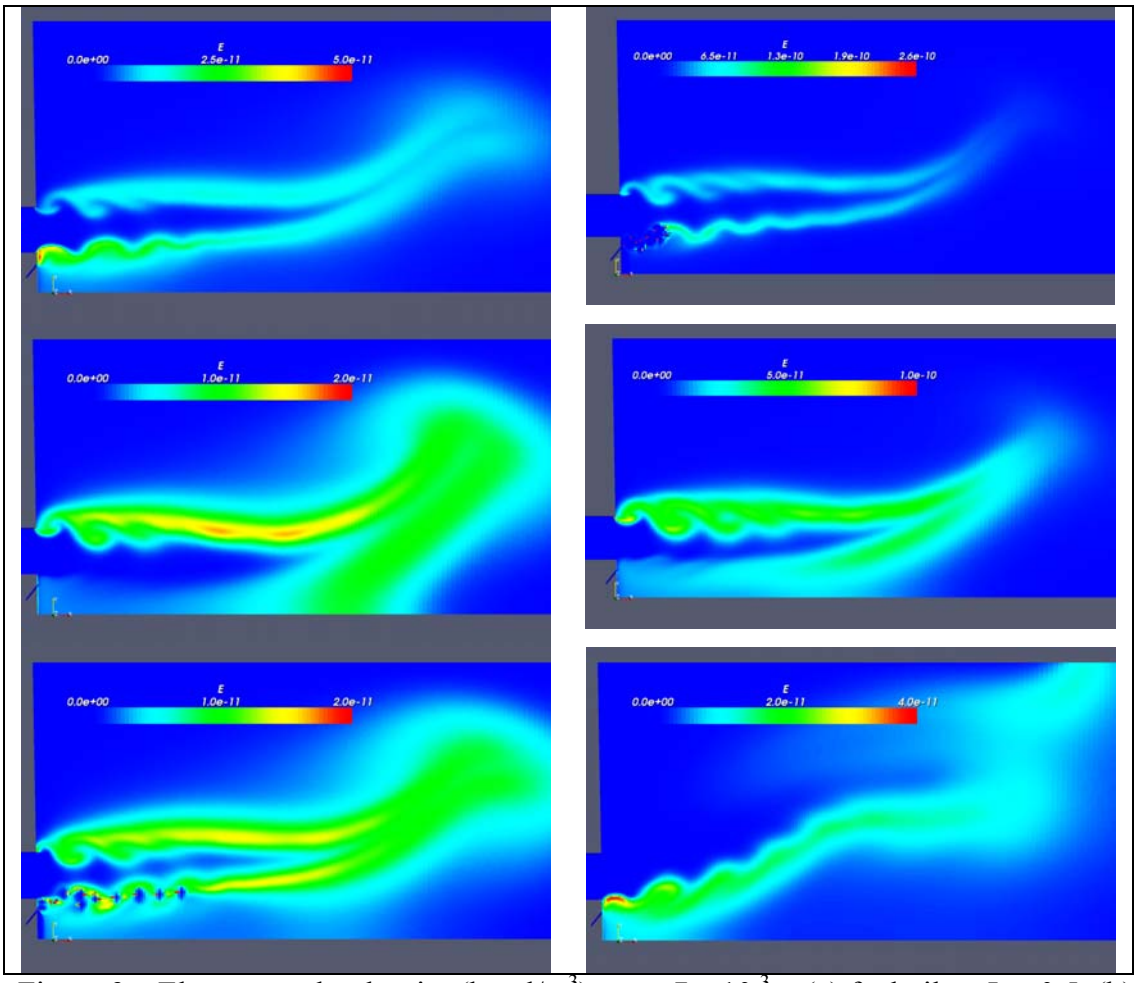

Figure 9 – Electron molar density (kmol/m^3) at t = 7 x 10^{-3} s, (a) fuel pilot, Φ = 0.5, (b) fuel pilot, Φ = 0.6, t = 6.85 x 10^{-3}(c) air pilot, Φ = 0.5, (d) air pilot, Φ = 0.6, (e) high mobility, Sc = 0.003, (f) combustor ignition

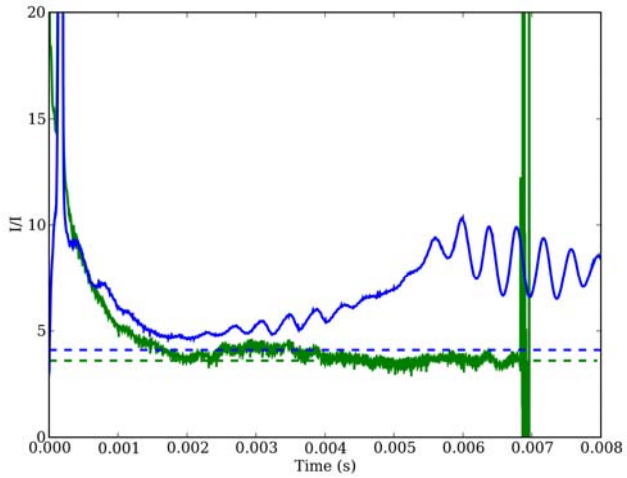

Figure 10 – The ratio of current at Φ = 0.6 to current at Φ = 0.5.
blue: no pilot; green: pilot; solid: simulation; dashed: experiment

Figure 11 shows the normalized pressure at a point near the outer recirculation zone. All 4 simulations show similar pressure time histories with two primary frequencies. As observed in experiments [e.g. Chorpening et. al. 2006], the peaks in pressure and current occur at similar frequencies, however the relative magnitudes are different.

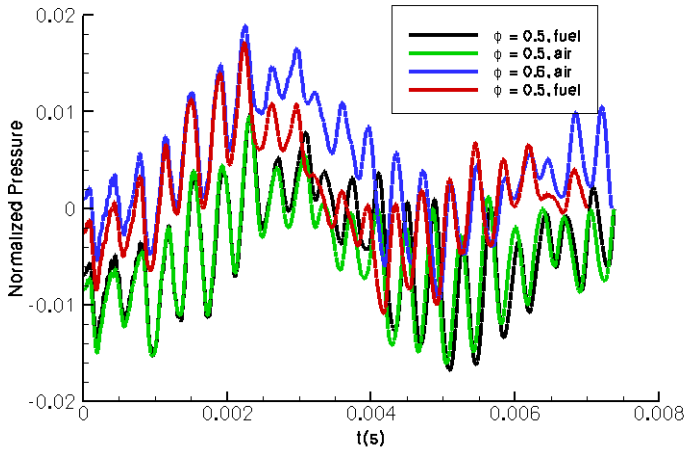

Figure 11 – Normalized Pressure $\left(\frac{p(t)}{p(0)}-1\right)$.

black: pilot, Φ = 0.5; green: no pilot, Φ = 0.5; blue: no pilot, Φ = 0.6, red: pilot Φ = 0.6.

The behavior of these four simulations seems to indicate that interaction of the pilot flow with the primary flow is not properly captured in this axisymmetric model, particularly the level of flame attachment/detachment. The smaller penetration distance of the fuel jet creates an unrealisticly high current carrier density in the immediate vicinity of the electrode. This is exaggerated by the fact that the jet acts uniformly in the azimuthal direction. In the unpiloted case, the symmetry of the jet is probably the cause of the detachment of the flame, leading to an unrealistically low current signal.

6. 3 Other Model Parameters

Figure 12 shows a comparison of the current history of simulations using the alternate ignition strategy, with an electrically insulated outer combustor wall and the baseline simulation (Φ = 0.5 and fuel piloting). During the initial development of the flame the current signal of the instulated and non-insulated wall are similar. As the flame moves away from the electrode, the current with the insulated boundary condition is lower than the grounded case, due to a lower field strength.

The flame structure using the alternate ignition strategy is quite different than the basedline flame structure based on the electron density contours (Figure 9f). Both current and pressure (Figure 13) illustrate these differences. In addition to having a lower current signal the alternate ignition simulation has a higher fluctuating pressure amplitude.

The next simulation involved increasing the mobility by reducing the electron Schmidt number from 0.006 to 0.003. The current history is shown in Figure 14 and indicates that an instability was triggered, though not catastrophic. The instability is also seen in the electron concentration (Figure 9e). The calculated current is generally higher than the baseline case, which is the expected behavior given larger attractive force of the electrons to the electrode.

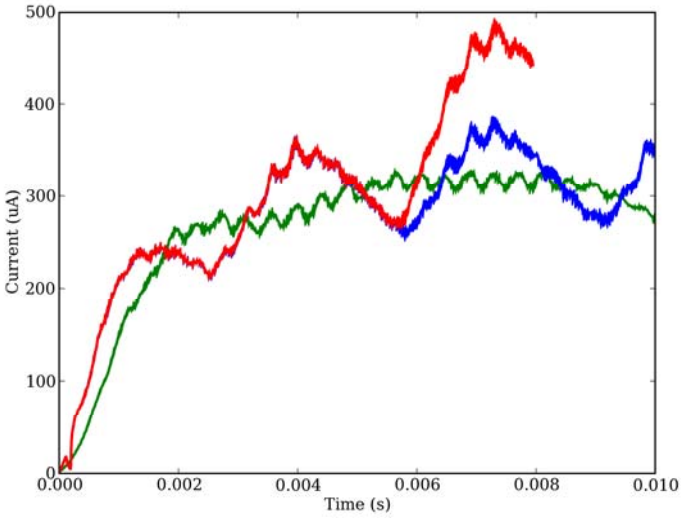

Figure 12 - Guard Current , piloted, Φ = 0.5
red: grounded combustor/injector ignition; blue: insulated combustor/injector ignition;
green: grounded combustor/combustor ignition

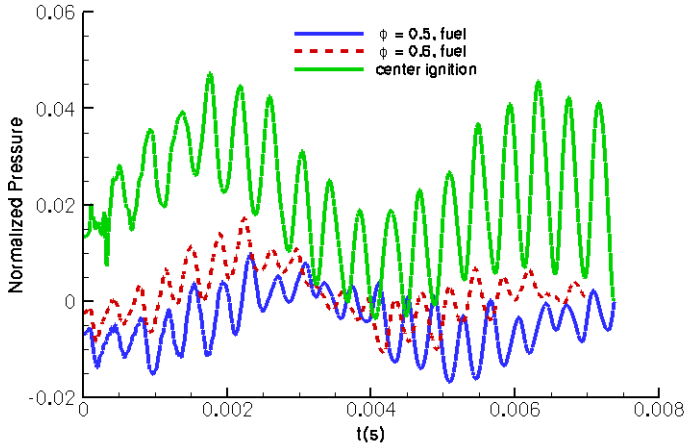

Figure 13 - Normalized Pressure
blue: pilot Φ = 0.5, red dashed: pilot Φ = 0.6, green: combustor ignition

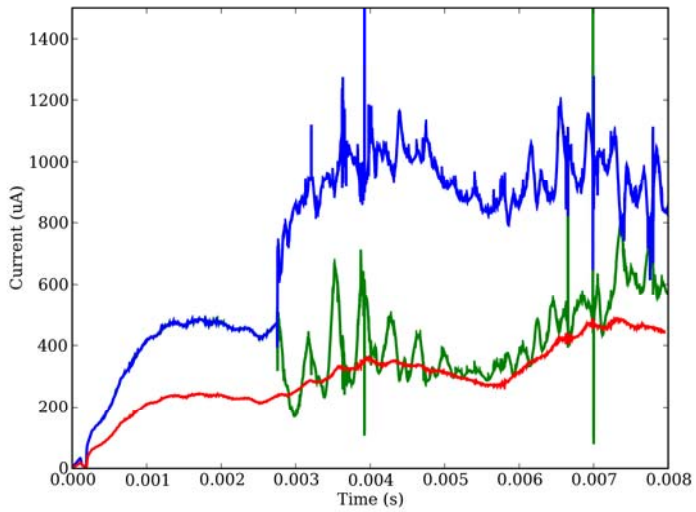

Figure 14 – Guard Current: pilot, Φ = 0.5
red: Sc = 0.006; green: Sc = 0.003, odd points; blue: Sc = 0.003, even points

6.4 Numerical Instability

The simulation with fuel piloting at equivalence ratio of 0.6 destabilized catastrophically (Figures 6 and 9b). One causes likely due to lack of convergence in predictor corrector loop. One possible cure would be to replace the predictor-corrector scheme with another non-linear iteration method which provide better coupling between the fields. This could include abandoning the segregated solution method, using the existing segregated algorithm as preconditioner for a Krylov method [Evans et. 2006] or using an alternative equation for the electrical potential with better mathematical properties [Crispel et. al. 2006]. These approaches might also have some benefits in computational efficiency and will be explored in a future work. The odd-even instability displayed the higher mobility simulation (Figure 14, Sc = 0.003) would suggest that the lack of convergence is a symptom as opposed to the root cause. This behavior could be caused by the method of upwinding the charged species flux.

At any face in the domain the species flux, F^*, can be written as:

$$F^* = \frac{u+u_d}{2}(C_R + C_L) - \left(\frac{|u+u_d|}{2} + D_{eff} \right)(C_R - C_L)$$

where, $u_d = -bz\nabla\phi$, is the drift velocity. The instability might be traced to the fact that the artificial diffusion, $|u+u_d|/2$, which is necessary to stabilize the iteration, will go to zero, when the drift velocity, of the electrons in particular, is balanced by the convective velocity. Unfortunately, this stagnation surface (line) can also intersect the flame, where large gradients in concentration exist and the due to lack of resolution of the flame, the artificial diffusion is particularly needed. One cure applied by [Gnoffo 1990] is to insure a finite amount of artificial dissipation is always added to the solution, i.e.:

$$F^* = \frac{u+u_d}{2}(C_R + C_L) - \left(\frac{|u+u_d|}{2} + D_0 + D_{eff} \right)(C_R - C_L) .$$

Preliminarily, we have selected a more dissipative approach by upwinding the convective and drift fluxes individually,

$$F^* = \frac{u+u_d}{2}(C_R + C_L) - \left(\frac{|u|+|u_d|}{2} + D_{eff} \right)(C_R - C_L) .$$

This form insures a finite artificial dissipation at the stagnation surface due to the balanced drift and convective velocities, but does not affect the behavior at a stagnation surface caused by both velocities going to zero.

The simulation using the alternative upwind flux function at Φ = 0.6 with fuel piloting was started from the solution using data before the amplitude of the instability became large (t=0.613). The resulting current signal is shown in Figure 15. The analogous signal for the high mobility (low Schmidt number) case is shown in Figure 16. This reformulation of the flux appears to have stabilized the system. More detailed analysis of this phenomena and comparison of the relative merits of the different solution approaches is left for a future work.

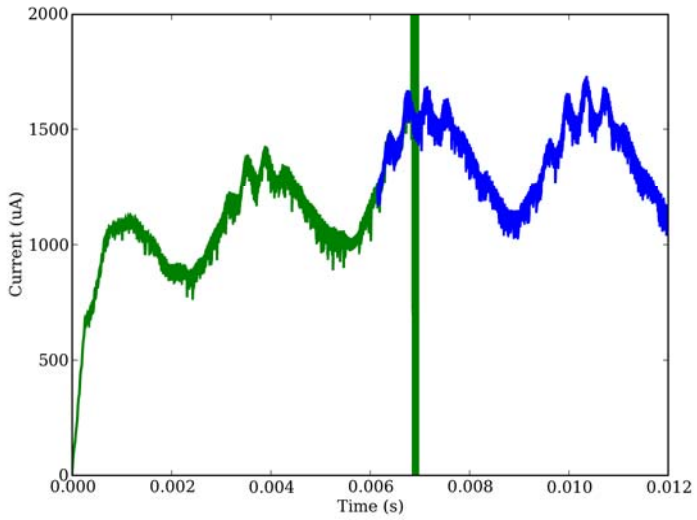

Figure 15 – Guard Current Φ = 0.6, fuel pilot
green: upwind using the net species velocity, blue: upwind fluxes individually

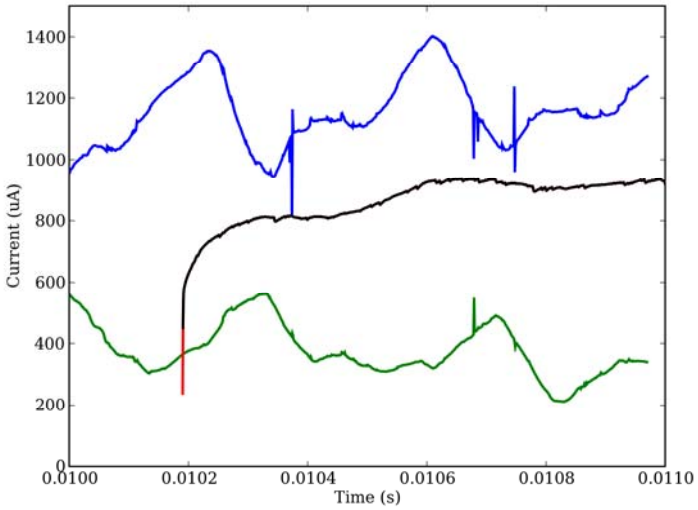

Figure 16 – Guard Current Φ = 0.5, Sc = 0.003
green: upwind using the net species velocity, blue: upwind fluxes individually

6.5 Revised Ion Production Rate

The simulations discussed above all used CCR rule based on the uncorrected rate expression, $k_{ion} = 2.51\times10^{11}\exp\left(-3.61\left(K\right)/T\right)cm^3/mol/s$.

The piloted, 0.5 equivalence ratio simulation was restarted at about 0.006 seconds using the revised expression,

$k_{ion} = 2.51\times10^{11}\exp\left(-856\left(K\right)/T\right)cm^3/mol/s$,

which reduced the CCR constant by about half (Figure 1). The calculated current is lowered (Figure 17), but still not to those observed experimentally. Refinement of the reaction model through the used of alternate recombination rates or extension of the model to include electron attachment to heavy molecules [Aithal et. al. 1999, Prager et. al. 2007], should further reduce difference between the simulated currents and measured currents.

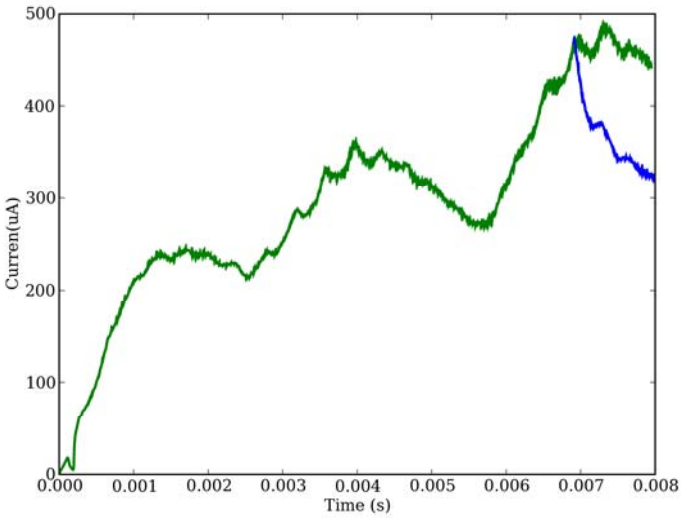

Figure 17 – Guard Current Φ = 0.5
green: CCR calculated with Ea = 3 K, blue: CCR calculated with Ea = 856 K

Conclusions

A sub-model has been developed to simulate the current produced from the transport of charged species in turbulent flames with an applied electric field. Quantitative agreement with experiment was not obtained, however the model does display similar sensitivity to flow and operating conditions as observed in experiments. The lack of quantitative agreement is not surprising given the many assumptions that were made in the formulation of the physical model, and the simplifications to the geometry and flow conditions in the construction of the numerical model. Better quantitative agreement should be possible with improvements to the ion model and/or the more detailed modeling of the primary combustion process.

Numerical instabilities were observed in two of the nine cases simulated. Several strategies to overcome the instability were suggested. A strategy of upwinding the drift flux and the convective flux separately appeared to damp the instability, but may be more diffusive than necessary. This issue will be revisited more thoroughly in future work.

Acknowledgement

The support of this work by U.S. DOE Turbines Program and Advanced Fossil Energy Research Program is gratefully acknowledged.

References

Aithal, S.M., White, A.R., and Subramaniam, V.V, 1999, "Kinetic Modeling of an Ionization Sensor for Combustion Processes", *AIAA 30th Plasmadynamics and Laser Conference*, AIAA P-99-3606.

Benson, K., Huckaby, E. D., Huckaby; Chorpening, B. T. and Straub, D.L. (2005), "Detection of Lean Blowout and Combustion Dynamics Using Flame Ionization", ASME Paper GT2005-68612.

Brown, R. C., and Eraslan, A. N., 1988, "Simulation of ionic structure in lean and close-to-stoichiometric acetylene flames", Combustion and Flame, vol. 73, pp.1-21.

Bukowski, J.D., Graves, D.B. and Vitello, P., 1996, "Two-dimensional fluid model of an inductively coupled plasma with comparison to experimental spatial profiles", Journal of Applied Physics, vol. 80, n. 5, pp.2614-2623.

Chorpening, B.T., Thornton, J. D., Huckaby, E. D. and Bensen, K., 2004, "Combustion Oscillation Monitoring Using Flame Ionization in a Turbulent Premixed Combustor", ASME Paper GT2004-53881.

Chorpening, B.T., Morris, M.L., Huckaby, E.D., Thornton, J.D., and Bensen, K.J., 2006, "Flame Ionization Distribution and Dynamics Monitoring in a Premixed Combustor", ASME Turbo Expo 2006, GT2006-9087 pp.9.

Crispel, P., Degond P. and Vignal, M.-H., 2005, "An asymptotically stable discretization for the Euler-Poison system in the quasi-neutral limit", Comptes Rendus Mathematique, vol. 341, is.5., pp. 323-328.

Eraslan, A. N., and Brown, R. C., 1988, "Chemiionization and Ion-Molecule Reactions in Fuel-Rich Acetylene Flames," *Combustion and Flame*, v. 74, pp. 19-37.

Evans, K.J., Knoll, D.A. and Pernice, M. 2006, "Development of a 2-D algorithm to simulate convection and phase transition efficiently", *Journal of Computational Physics*, Volume 219, Issue 1, Pages 404-417.

Fialkov, A.B., "Investigations on Ions in Flames." Progress in Energy Combust. Science, v23, 1997, pp. 399-528.

Gregory P. Smith, David M. Golden, Michael Frenklach, Nigel W. Moriarty, Boris Eiteneer, Mikhail Goldenberg, C. Thomas Bowman, Ronald K. Hanson, Soonho Song, William C.

Gardiner, Jr., Vitali V. Lissianski, and Zhiwei Q in http://www.me.berkeley.edu/gri_mech/.

Gnoffo, P. A., 1990, "An Upwind-Biased, Point-Implicit Relaxation Algorithm for Viscous, Compressible Perfect-Gas Flows", NASA Technical Paper 2953, pp. 68.

Goodwin, D.G., 2006, Cantera v.1.7, www.cantera.org.

Hagelaar, G., 2000, "Modeling of Microdischarges for Display Technology", Ph.D. Thesis, Technische Universiteit Eindhoven.

Hayt, 1981, *Engineering Electromagnetics*, McGraw-Hill.

Holm, T., 1999, "Aspects of the Mechanism of the Flame Ionization Detector." *Journal of Chromatography A, v842*, pp. 221-227.

Hu, J., Rivin, B., and Sher, E., 2000, "The effect of an electric field on the shape of co-flowing and candle-type methane-air flames", *Experimental Thermal and Fluid Science*, vol.21, pp.124-133

Jasak, H., Weller, H.G., and Nordin, N., 2004, "In-cyllinder CFD Simulation Using a C++ Object-Oriented Toolkit", SAE Paper 2004-01-0110.

Jones, F. L. and Becker, P. M., 1972, "A Mathematical Model of the Opposed-Jet Diffusion Flame: Effect of an Electric Field on Concentration and Temperature Profiles", *Combustion and Flame, 19,*

Lilly, J. 2007, "One-Dimensional Computer Modeling of Electrical Conductivity through Natural Gas and Syngas Flames", M.S. Thesis, West Virginia University.

Mehresh, P., Souder, J., Flowers, D., Riedel, U. and Dibble, R.W. 2005, "Combustion timing in HCCI engines determined by ion-sensor: experimental and kinetic modeling", *Proceedings of the Combustion Institute*, v. 30, issue 2, January 2005, pp 2701-2709.

Prager, J. 2005, "Modeling and Simulation of Charged Species in Lean Methane-Oxygen Flames", Ph.D. Thesis, Universität Heidelberg.

Penderson, T. and Brown, R. C., 1993, "Simulation of Electric Field Effects in Premixed Methane Flames", *Combustion and Flame 94:433-448*.
Poinsot, T. and Veynante, D., 2001, *Theoretical and Numerical Combustion*, Edwards, pp.473.

OpenFOAM, 2006, *OpenFOAM version 1.3*, www.openfoam.org.

Quin, Z., Lissianski, V., Huizing Y., Gardiner, W.C., Davis, S.G. and Wang, H., 2000, "Combustion Chemistry of Propane: A Case Study of Detailed Reaction Mechanisms Optimization", Proceedings of the Combustion Institute, vol. 28, pp.1663-1669.

Sakhrieh, A., Lins, G., Dinkelacker, F., Hammer, T., Leipertz, L., and Branston, D.W., 2005, "The influence of pressure on the control of premixed turbulent flames using an electric field", v.143, issue 3, pp. 313-322

Sidwell, T., Richards, G., Casleton, K., Straub, D., Maloney, D., Strakey, P., Ferguson, D., Beer, S., and Woodruff, S., 2006, "Optically Accessible Pressurized Research Combustor for CFD Model Validation," AIAA Journal, 44 (3), pp. 434-443.

Selle, S. and Riedel, U., 2000, "Transport Coefficients of Reacting Air at High Temperature", *38th Aerospace Sciences Meeting and Exhibit*, AIAA P 2000-0211.

Straub, D. L., Thornton, J. T., Chorpening, B. T., Richards, G. A., 2002, "In-Situ Flame Ionization Measurements In Lean Premixed Natural Gas Combustion Systems", presented at the Western States Section/Combustion Institute Spring Meeting, San Diego, CA, March 25-26.

Subramaniam, V.V, 2005, *Personal Communication*.

Sveha, R. A., 1995, "Transport Coefficient for the NASA Lewis Chemical Equilibrium Program", NASA Technical Memorandum 4647.

Thornton, J.D., Richards, G.A., and Robey, E., 2000, "Detecting Flashback in Premix Combustion Systems", presented at the American Flame Research Committee International Symposium, Newport Beach, California, September 17-21.

Weller, H.G., 1998, G. Tabor, A.D. Gosman, C. Fureby, "Application of a Flame-Wrinling LES Combustion Model to a Turbulent Mixing Layer", Prof. Comb. Inst. 27 (1998) p.889.

Weller, H.G., 1993, "The Development of a New Flame Area Combustion Model Using Conditional Averaging", Thermo-Fluid Section Report TF/9307, Imperial College of Science Technology and Medicine.